The Comb-Type Slow-Wave Structure For TWM Applications*

By F. S. CHEN

(Manuscript received December 5, 1963)

The space harmonic analysis of the dielectrically loaded comb structure as used in traveling-wave masers (TWM) is presented. The frequency-phase characteristics (the ω-β diagrams) are computed by regarding each finger of the comb structure as a capacitive loaded transmission line. The impedance of the line is based on the space harmonic analysis. Computed data are found to be in agreement with experimental results and, in particular, it is confirmed that the ω-β relation depends very critically on certain dimensions of the dielectric loading. The results of the analysis are used to derive prescriptions for the design of dielectrically loaded TWM comb structures, especially of structures with low group velocity which are suitable to provide simultaneously large gain and large instantaneous bandwidth.

I. INTRODUCTION

The comb-type structure has been used successfully as a slow-wave structure for traveling-wave masers (TWM).[1] In a TWM the small-signal gain in db is inversely proportional to the group velocity. Generally the gain obtainable from present maser materials is small. Therefore, a great deal of effort in developing a TWM is concerned with deriving a comb structure design with small group velocity at the frequency of interest. Both the group velocity and the passband of the comb structure can be found from the ω-β diagram. The shape of the ω-β diagram of the comb structure loaded with "masing" crystal depends very critically on the various dimensions of the structure as well as of the crystal. In this paper, an analysis of the comb structure will be presented. It should serve as a guide for a reasonably accurate determination of the dimensions of the comb structure, of the active maser material and of other dielectrics which give rise to a required ω-β diagram. Some additional

* This work was supported in part by the U. S. Army Signal Corps under Contract No. DA 36-039-SC-89169.

experimentation may be needed in practice for small corrections of the resulting ω-β characteristic.

Various tape structures with the tapes perpendicular to the direction of signal propagation have been proposed and analyzed[2,3,4,5] in the past. The space harmonic analysis originally introduced by Fletcher[2] was used to obtain the ω-β diagrams of these tape structures. It assumes no RF field components in the direction of the tape (TEM wave approximation); that is, the tape can be regarded as a transmission line supporting the TEM wave in the direction transverse to the direction of signal propagation. An impedance matching condition for the TEM lines in the transverse plane can be derived (transverse resonance). The resulting equation implicitly contains the ω-β relation. The authors mentioned treated only the case where the structure is immersed in a uniform dielectric, that is, mostly vacuum. For the TWM application, the structure is alway partially loaded with dielectric and the TEM approximation no longer holds. However, when the structure is nearly filled with dielectrie, as in TWM's for a large gain and simultaneously large instantaneous bandwidths,[6] one finds that the TEM approximation can also be successfully used to calculate the ω-β diagram of the dielectric-loaded tape structures. An "effective dielectric constant" is then defined to take into account the fact that the structure is only partially loaded with dielectric. This approach was used in earlier calculations of the upper and lower cutoff frequencies of the comb structure by Harris, DeGrasse and Schulz-DuBois.[7] The analysis to he presented here extends their work to cover the entire ω-β diagram.

The ω-β diagram of the comb structure[1] and the "Karp structure"[8] for TWM applications had also been discussed previously, using the equivalent circuit method. However, the field analysis to be presented here gives a more detailed understanding of the structure. For instance, the filling factor of the active crystal and the performance of the isolator embedded in the structure are readily obtained by this analysis.

In the next three sections, the ω-β diagram of the comb strueture, the impedance of the tapes (or fingers) and the effective dielectric constant will be derived. This is followed by a more detailed discussion of various properties of the comh structurc, including the techniques available for reducing the bandwidth of the passband, higher-order transmission bands of the strueture and practical design considerations. The calculations are usually compared with experiments, and they are found to be in good agreement.

The impedance of the finger and the effective dielectrie eonstant are defined as a function of θ, the phase angle between adjacent fingers. The phase angle θ, or equivalently the phase propagation constant β, are

related to the frequency ω by the ω-β relation which is obtained from the transverse resonance matching condition. Only the ruby-loaded comb structure is treated here up to and including numerical details. It is easily possible, however, to extend the same type of analysis to other types of tape structures. This is particularly easy since both the impedance and the effective dielectric constant are evaluated here as functions of θ and not of ω.

II. THE ω-β DIAGRAM

Let us consider first a comb structure without dielectric loading (empty comb). The open end of the fingers has fringing electric fields terminating at the surrounding conductors. The effect of these fields can be expressed by a capacitance C (Fig. 1) which in general is a function of θ, $C = C(\theta)$, where θ is the phase angle between the adjacent fingers and takes values from zero to π radians over the passband. It will be assumed that the RF electric and the magnetic fields vanish in the direction of fingers (y direction) except at the finger tip. Then the finger can be regarded as a TEM transmission line with a characteristic impedance K and supporting a wave propagation in the y direction with velocity c, the velocity of light in free space. K is a function of θ, $K = K(\theta)$. At the finger tip ($y = h$), the impedance looking in $+y$ and $-y$ directions must have the same magnitude and the opposite sign; therefore there exists a matching condition

$$\frac{1}{\omega C(\theta)} = K(\theta) \tan \frac{\omega h}{c}. \tag{1}$$

According to this equation, the grounded finger presents an inductive reactance at the finger tip. The length of the finger h is therefore limited by

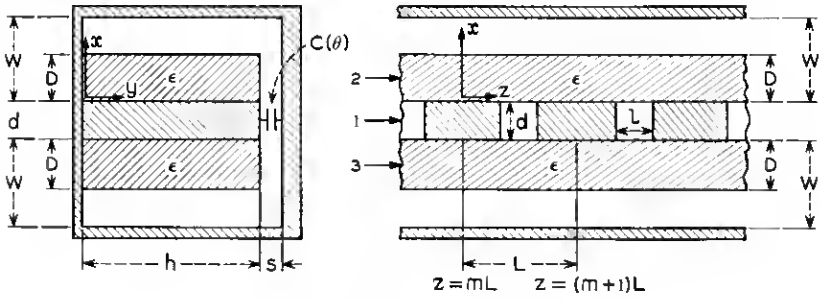

Fig. 1 — Cross sections of the comb structure.

$$(m - 1)\pi < \omega h/c < (m - \tfrac{1}{2})\pi, \qquad m = 1, 2, 3, \cdots . \tag{2}$$

For a given θ, one can find the frequeney from (1), provided the functions $K(\theta)$ and $C(\theta)$ are known, and in this way the ω-β diagram (or ω-θ diagram) may be derived. For $m = 1$, the finger acts essentially as a quarter-wave resonator and (1) gives the lowest passband for a given geometry of the eomb strueture. For $m = 2$, the finger behaves as a three-quarter wave resonator and the next higher passband appears. Thus the comb strueture provides a series of passbands separated by stop bands.

When the eomb strueture is partially loaded with dielectrie as in Fig. 1, there appear components of RF fields in the y direction, and the finger no longer behaves as a TEM line. However, when the structure is almost completely loaded with the dieleetrie, the fields are again approximately TEM waves in the y direction. We will adopt this TEM approximation for the loaded structure and modify the impedance K and the propagation eonstant ω/c of (1) by a faetor $\sqrt{\epsilon(\theta)}$. $\epsilon(\theta)$ is ealled tbe effeetive dieleetrie eonstant and it will be defined more rigorously in Section IV. Then the dispersion equation for the loaded comb can be expressed as

$$\frac{1}{\omega C(\theta)} = \frac{K(\theta)}{\sqrt{\epsilon(\theta)}} \tan \frac{\omega h \sqrt{\epsilon(\theta)}}{c} \tag{3}$$

for the case where the structure is loaded with dieleetrie of uniform thiekness from $y = 0$ to $y = h$ as in Fig. 1. For simplieity $K(\theta)$, $C(\theta)$ and $\epsilon(\theta)$ will be abbreviated as K, C and ϵ from here on. The TEM approximation offers a further advantage, sinee it enables one to analyze the various "finger tip loadings" in a simple way.

It turns out that, in practical realizations of the comb structure, the fringe capaeity C is always small, so that $\omega h\sqrt{\epsilon}/c$ is close to $(m - \frac{1}{2})\pi$ with $m = 1, 2, 3, \cdots$. Hence (3) can be simplified by defining a quantity Δh through

$$\omega \sqrt{\epsilon}(h + \Delta h)/c = (m - \tfrac{1}{2})\pi. \tag{4}$$

Substituting (4) into (3) and using the fact that $\Delta h \ll h$, one obtains

$$\Delta h \doteq (KCc/\epsilon) \tag{5}$$

where it should be noted that Δh is also a function of θ. Equation (4) becomes

$$(2m - 1)\frac{\lambda}{4} \doteq \sqrt{\epsilon}\left(h + \frac{KCc}{\epsilon}\right) \tag{6}$$

where $\lambda = c/f$ is the free-space wavelength. For the empty comb, the ω-β diagram can be obtained from (6) by letting $\epsilon = 1$. Equation (6) states that, in the passbands, the finger length h plus the correction due to the fringe capacitance at the finger tip should be $(2m - 1)\lambda/4$ when measured with the scale $\sqrt{\epsilon}$.

III. IMPEDANCE OF THE FINGER, $K(\theta)$

The admittance of a single finger as a TEM line is a somewhat abstractly defined quantity. One considers transmission lines having the cross section shown in Fig. 1(b), but without dielectric and infinitely long in the $\pm y$ directions, or alternatively suitably terminated. On this set of identical transmission lines one considers waves of equal amplitude traveling, for example, in the $+y$ direction and phased by θ between adjacent lines in the $+z$ direction. Under these conditions, the admittance of a single finger is defined as the ratio of current to voltage on a finger and is a function of θ.

Consider a comb structure as in Fig. 1, but without the dielectric and with the structure divided into three regions as shown. Then the current on a finger is the sum of the current on the surface of the finger in region 1 (between the fingers) and the current on the surface of the finger in regions 2 and 3. Thus the admittance of the finger is the sum of two admittances:

$$Y(\theta) = Y_1(\theta) + Y_2(\theta) \tag{7}$$

where $Y_1(\theta)$ is the admittance due to the current on the surface of the finger in the region 1 and $Y_2(\theta)$ is the admittance due to the current on the surface of the finger in the regions 2 and 3.

The current on the finger can be found by a line integral of the RF magnetic fields, which in turn can be found by matching boundary conditions in the x-z plane.

The potential on the mth finger may be written as

$$V_m = Ve^{-jm\theta} \tag{8}$$

where θ is again the phase angle between the adjacent fingers and may vary from 0 to π. Then, as will be shown in Appendix A, the potential along the z axis between the mth and the $(m + 1)$th finger can be expressed as

$$V(\theta,z) = Ve^{-j(m+\frac{1}{2})\theta}\left[g(z)\cos\frac{\theta}{2} - jf(z)\sin\frac{\theta}{2}\right] \tag{9}$$

where $g(z)$ and $f(z)$ specify the symmetric and the antisymmetric part of the potential distribution respectively. $g(z)$ is also the potential distribution when $\theta = 0$, and $f(z)$ is also the potential distribution when $\theta = \pi$. It should be added that the representation of the θ-dependent potential distribution by a combination of θ-independent symmetric and antisymmetric functions, $g(z)$ and $f(z)$, is at best a good approximation or, to use a more appropriate term, a guess. The representation is strictly correct only for $\theta = 0$ and $\theta = \pi$. However, it is bound to be a good approximation near $\theta = 0$ and near $\theta = \pi$ where one of the functions dominates. The calculations show that the detailed shape of the potential distribution assumed is of little influence in the midband region near $\theta = \pi/2$ and in fact up to $\theta = \pi$. It is in this sense that the expression into a symmetric and an antisymmetric part, which is a powerful tool in other electromagnetic problems, is justified here.

The RF electric field on the z axis becomes

$$\begin{aligned} E_z &= 0, \qquad mL - \frac{L-l}{2} < z < mL + \frac{L-l}{2} \\ &\qquad\qquad\qquad\qquad\qquad\qquad\qquad\qquad \text{(on the fingers)} \\ E_z &= -\frac{\partial V}{\partial z}, \qquad (m+\tfrac{1}{2})L - \frac{l}{2} < z < (m+\tfrac{1}{2})L + \frac{l}{2} \\ &\qquad\qquad\qquad\qquad\qquad\qquad\qquad\qquad \text{(between fingers).} \end{aligned} \tag{10}$$

The E_z field in region 2, E_{z2}, may be expressed by a space harmonic or generalized Fourier sum

$$E_{z2} = \sum_{n=-\infty}^{\infty} F_n \sinh \beta_n(W - x) e^{-j\beta_n z} e^{jky} \tag{11}$$

where $\beta_n L = \theta + 2n\pi$, W is the height of the waveguide as shown in Fig. 1, and F_n is the amplitude of the nth space harmonic component. Each term of the sum is the electric field of a TEM solution to Maxwell's equations, and the z dependence, $\exp(-j\beta_n z)$, assumes periodicity of the resulting field pattern from finger to finger as required by (8). The as yet unknown amplitude coefficients F_n are determined by letting $x = 0$ in (11) and equating the resulting expression with the field on the z axis (10). Thus,

$$F_n = -\frac{Ve^{-j(m+\frac{1}{2})\theta}}{L \sinh \beta_n W} \int_{(m+\frac{1}{2})L-(l/2)}^{(m+\frac{1}{2})L+(l/2)} \left[g' \cos\frac{\theta}{2} - jf' \sin\frac{\theta}{2} \right] e^{j\beta_n z} dz \tag{12}$$

where $g' = dg/dz$ and $f' = df/dz$. The current on the surface of the mth

finger facing regions 2 and 3 can be found from the line integral of the z component of the RF magnetic field there, and finally Y_2 becomes

$$Y_2(\theta) = 2Y_0 \frac{L-l}{L} \sum_{n=-\infty}^{\infty} (-1)^n \frac{\sin \frac{\beta_n(L-l)}{2}}{\frac{\beta_n(L-l)}{2}} \coth \beta_n W \times \left[\cos \frac{\theta}{2} \int_{(L-l)/2}^{(L+l)/2} g' \sin \beta_n z \, dz + \sin \frac{\theta}{2} \int_{(L-l)/2}^{(L+l)/2} f' \cos \beta_n z \, dz \right] \tag{13}$$

where $Y_0 = \frac{1}{377}$ mho.

In the case of constant-field approximation, as has been assumed by Fletcher,[2]

$$\begin{aligned} g &= 1 \\ f &= (2z/l) - (L/l). \end{aligned} \tag{14}$$

The integration in (13) can be readily performed. For the case where $L - l = L/2$ and $d = l$ (square finger cross section),

$$\frac{Y_2(\theta)}{Y_0} = 2 \sin \frac{\theta}{2} \sum_{n=-\infty}^{\infty} (-1)^n \left(\frac{\sin \frac{\beta_n L}{4}}{\frac{\beta_n L}{4}} \right)^2 \coth \beta_n W. \tag{15}$$

$Y_1(\theta)$ becomes, in the same constant-field approximation

$$\frac{Y_1(\theta)}{Y_0} = 4 \frac{d}{L} \sin^2 \frac{\theta}{2}. \tag{16}$$

The impedance of a finger $K(\theta) = (Y_1(\theta) + Y_2(\theta))^{-1}$ in the constant-field approximation is plotted in Fig. 2 in dashed lines as a function of θ/π for $W/L = 1.25$ and 0.75.

The constant-field assumption does not take into account the singularity in the field at the corner of the finger. It will be shown later that the calculated ω-β diagram using the impedance thus obtained disagrees severely with the measured one for $\theta < 0.5\pi$. Harris et al.[7] used the constant-field approximation for region 1 only and assumed the field produced by an infinitely thin tape for regions 2 and 3. This will be referred to as the thin-tape approximation. The calculation used conformal mapping and it is applicable directly only for $\theta = 0$, $\pi/2$ and π. The thin-tape approximation assumes a 180° singularity at the corner of the finger and thus exaggerates the actual 90° singularity there. A further difficulty in

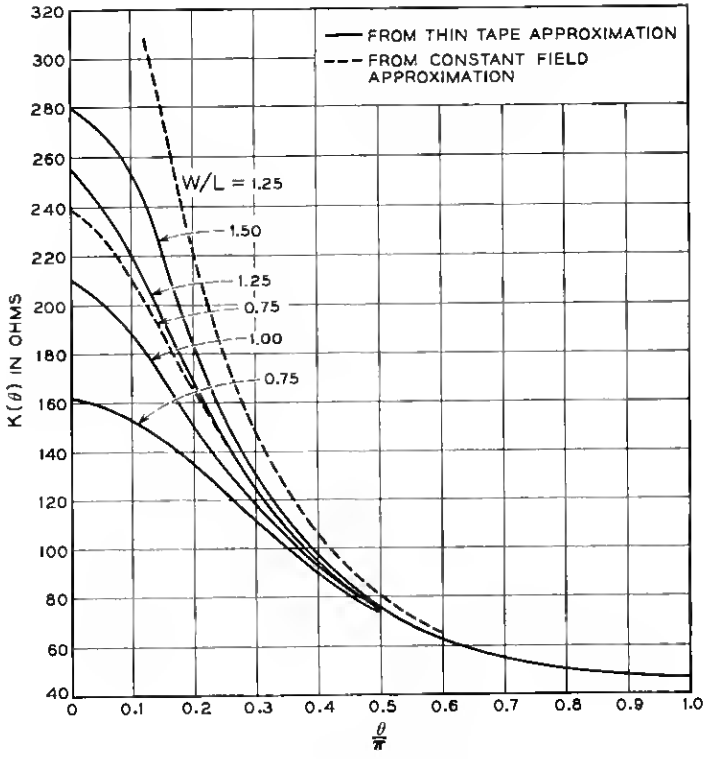

Fig. 2 — The impedance of the finger vs θ. It is assumed that $L - l = l = d$.

this approach is that the fields on the boundaries between the regions 2, 3 and the region 1 are not matched.

A third alternative would be to base the calculations on experimental data. The potential distribution functions $g(z)$ and $f(z)$ in (9) may be measured directly with a large scale two-finger model in an electrolytic tank. This is probably the most reliable method, although data are obtained with only limited accuracy and only numerically. In addition, the data are applicable directly with good accuracy only for $\theta = 0, \pi$.

The second (thin-tape) approximation will be used here, and it will be extended to cover the whole range of θ. With the thin-tape approximation, the functions g and f, which specify the potential distribution along the z-axis, for $\theta = 0$ and π respectively, can be found by Schwarz-Christoffel transformation. They have a quite complicated form involving elliptic functions, and therefore the integrals in (13) are difficult to

evaluate. Fortunately, at $\theta = 0$, $\pi/2$ and π, $K(\theta)$ can be found directly by Schwarz-Christoffel transformations without resort to (13). One can arrive at a good approximation of $Y_2(\theta)$ for the whole passband of the structure from (13) and the knowledge of Y_2 at $\theta = 0$, $\pi/2$ and π without evaluating the integral. The procedure is described in Appendix B, and the result is shown in Fig. 2 with solid lines for various values of W/L. Both the constant-field and the thin-tape approximations give about the same $K(\theta)$ for $\theta \geqq \pi/2$ but there is a large difference near $\theta = 0$. It will be shown later that $K(\theta)$ resulting from the thin-tape approximation yields a reasonably good agreement with experimental data.

IV. The Effective Dielectric Constant $\epsilon(\theta)$

If the comb is not entirely immersed in an isotropic medium, some RF field components appear in the direction of the fingers. The TEM assumption which has been used in Section II no longer holds. However, if the medium is only slightly nonuniform, the TEM assumption is still a good approximation. Fortunately, TWM's designed for high gain and large instantaneous bandwidth are so heavily loaded with an active crystal that the TEM approximation is reasonably valid and may be used in the structure analysis. In this section, an effective dielectric constant is defined. It is a function of θ — that is, of the details of the RF electric field configuration. At a particular value of θ, the effective dielectric constant of $\epsilon(\theta)$ is defined as the dielectric constant of a *uniform* medium filling the same comb structure, which results in the same total charge per comb finger as that produced by the true, incomplete dielectric loading (this definition is meaningful only for heavy dielectric loading such that the TEM approximation holds). It is obvious that this quantity $\epsilon(\theta)$ is a very helpful one for the analysis.

Referring to Fig. 1, a slab of dielectric of thickness D is placed in the regions 2 and 3. Its dielectric constant is assumed to be isotropic and equal to ϵ. TEM-type solutions of Maxwell's equations are assumed in regions 2 and 3, both inside and outside the dielectric slab. The components of the field vary as

$$\exp\left[\pm\beta_n x - jky - j\beta_n z\right]$$

where k is the plane wave propagation constant for the respective media. Boundary conditions have to be matched at $x = 0$, D and W in the y-z plane. The constant-field approximation expressed in (14) is explicitly used for the boundary condition at $x = 0$.

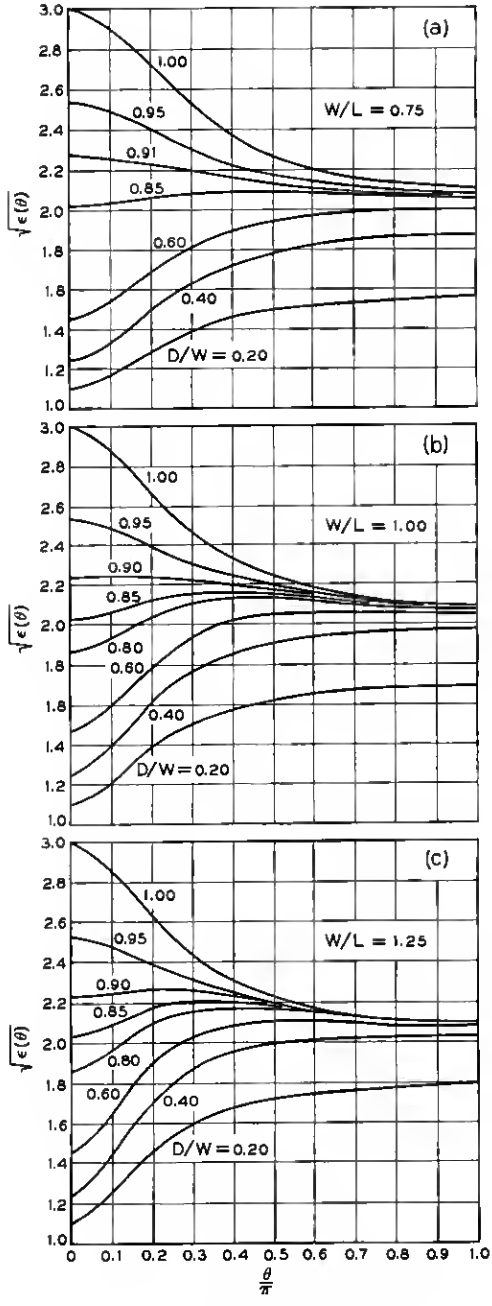

Fig. 3 — Square root of the effective dielectric constant vs θ. It is assumed that $L - l = l = d$, and $\epsilon = 9$.

Then the charge per unit length on a finger is given by

$$Q = 2\epsilon \int_{-(L-l)/2}^{(L-l)/2} E_{x2}dz + 2\int_{0}^{-d} E_{z1}dx \tag{17}$$

where E_{x2} is the x component of the electric field in region 2 at $x = 0$ and E_{z1} is the z component of the electric field in region 1. An effective dielectric constant $\epsilon(\theta)$ is now defined by requiring the same amount of charge Q to exist on the finger as if the whole structure were immersed in a medium of dielectric constant $\epsilon(\theta)$. The resulting formula can be given for combs with rectangular fingers; however, for simplicity, only the result for equally spaced square fingers ($L - l = d = L/2$) is given here

$$\epsilon(\theta) = \frac{\sin\frac{\theta}{2} + \frac{\epsilon}{2}\sum_{n=-\infty}^{\infty}(-1)^n\left(\frac{\sin\frac{\beta_n L}{4}}{\frac{\beta_n L}{4}}\right)^2 \times \left(\frac{1 + \epsilon\coth\beta_n(W-D)\coth\beta_n D}{1 + \epsilon\coth\beta_n(W-D)\tanh\beta_n D}\right)\tanh\beta_n D}{\sin\frac{\theta}{2} + \frac{1}{2}\sum_{n=-\infty}^{\infty}(-1)^n\left(\frac{\sin\frac{\beta_n L}{4}}{\frac{\beta_n L}{4}}\right)^2\coth\beta_n W} \tag{18}$$

The result of machine computations of $\epsilon(\theta)$ using (18) and assuming a dielectric constant of the loading dielectric of $\epsilon = 9$ (approximately the value of ruby) is shown in Fig. 3(a), (b), and (c). To facilitate other computations which will be discussed later, the square root $\sqrt{\epsilon(\theta)}$ is shown in these graphs rather than $\epsilon(\theta)$. For a fairly complete loading ($D/W > 0.8$), $\epsilon(\theta)$ approaches 5 near $\theta = \pi$. Near $\theta = 0$, $\epsilon(\theta)$ varies widely, depending on D/W. This can be understood by noting that near $\theta = \pi$ the RF fields concentrate near the fingers and hence $\epsilon(\theta)$ is little changed by a change in the width of the air gap near the waveguide wall. On the other hand, near $\theta = 0$ more of the fields reach the waveguide wall. Thus the width of the air gap there affects the magnitude of $\epsilon(0)$ more drastically than that of $\epsilon(\pi)$.

V. PROPERTIES OF THE COMB STRUCTURE

With the knowledge of $K(\theta)$, $C(\theta)$ and $\epsilon(\theta)$, one can calculate the ω-β diagram of both the empty and the loaded comb structure. The calculation reveals a number of interesting properties of the comb struc-

ture and also suggests various techniques for narrowing the passband of the structure.

5.1 *Empty Comb Structure*

As a maser structure, the comb is always loaded with one or more dielectrics. However, the study of the empty comb is of some interest to us, since it offers the possibility of checking the accuracy of our impedance calculations by measurements.

The fringe capacitance $C(\theta)$ for $\theta = 0$, and $\theta = \pi$ has been measured in the electrolytic tank. Values for $C(0)$ and $C(\pi)$ are shown in Fig. 4. They were obtained by resistance measurements on a large scale model of a comb finger in a tank. The values are plotted versus the distance between the finger tips and the opposite waveguide wall, s. The data are valid for fingers of square cross section, $L/2 \times L/2 = 0.040 \times 0.040$ inch, spaced center-to-center by $L = 0.08$ inch and contained in a housing of width $2W + L/2 = 0.240$ inch (aspect ratio $W/L = 1.25$). It should be mentioned here that these data can be applied to dimensions other than those indicated if one observes two facts. First, if all linear dimensions are scaled simultaneously by some factor, the capacity is scaled by the

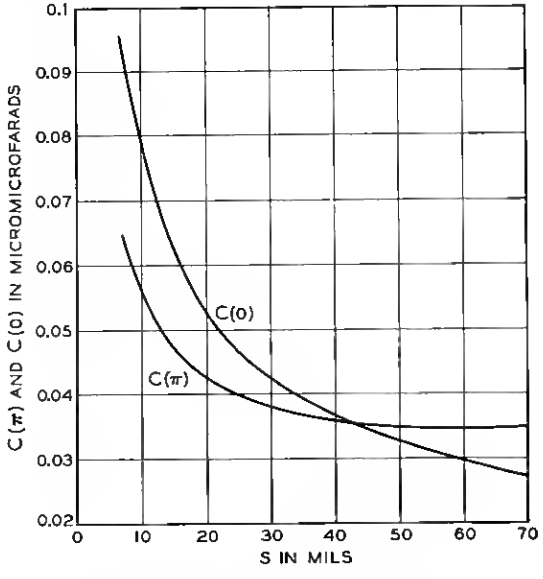

Fig. 4 — The fringe capacitance at $\theta = 0$ and $\theta = \pi$ vs the spacing between the finger tip and the waveguide wall for the case where $L = l = t = d = 0.040$ inch.

same factor. Second, experience has shown that the fringe capacity is a very slow function of the ratio W/L; no noticeable errors were found when these capacity values were used for W/L values ranging from 0.75 to 1.5. Unfortunately, $C(\theta)$ for θ other than 0, $\pi/2$ and π cannot be measured in a simple tank model. However, some indication of how $C(\theta)$ changes with θ may be obtained experimentally. One would start with a measured dispersion curve of an empty comb; one would assume that the values $K(\theta)$ in Fig. 2 for the thin-tape approximation are sufficiently accurate; then (1) offers a possibility of evaluating experimental values of $C(\theta)$. In practice it turns out, however, that this approach does not yield values $C(\theta)$ of sufficient accuracy to determine the exact shape of the $C(\theta)$ function.

In Fig. 5, calculated dispersion curves of several empty comb structures with dimensions as shown are given in solid lines. The calculation is based on $K(\theta)$ of Fig. 2 using the thin-tape approximation. $C(\theta)$ is assumed to change linearly with θ from $\theta = 0$ to $\theta = \pi$. Measured points of the dispersion curves are also shown in Fig. 5. The measurements and calculation agree well.

One case of a dispersion curve calculated by using $K(\theta)$ from the constant-field approximation is also shown in Fig. 5 by the dashed line. It deviates considerably from the measured points for $\theta < 0.5\ \pi$.

One may conclude that both the impedance of a finger calculated by using the thin-tape approximation and the assumption that $C(\theta)$ changes linearly with θ are sufficiently accurate for the present analysis.

The passband of the empty structure can be narrowed by reducing the width of the waveguide housing $2W + d$. Then the impedance values $K(\theta)$ at $\theta = \pi$ approach each other more closely and so do the Δh values at $\theta = 0$ and $\theta = \pi$. From (6), one readily sees that a narrower passband results.

5.2 *Loaded Comb Structure*

In this section, the discussion is restricted to the case of dielectric loading on both sides of the comb. Both loading slabs are parallelepipeds of equal thickness D. Both slabs cover the full finger height from the root to the tip, i.e., the height h of the fingers is also that of the loading slab. In addition, a comb of equally spaced square cross section fingers ($L - l = l = d$) is assumed.

Since (3) is only an approximation and also since the dielectric constant of ruby is neither a scalar nor exactly 9, one cannot expect to obtain a close quantitative agreement between the measured and the

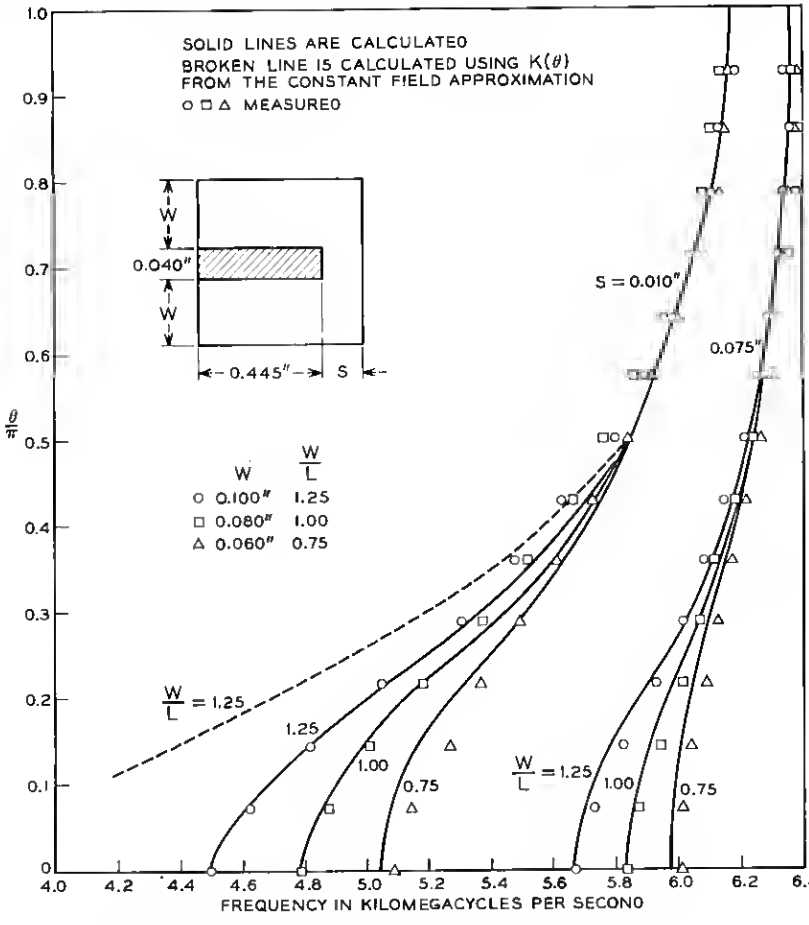

Fig. 5 — Calculated and the measured ω-β diagram of the empty comb. $L - l = l = d = 0.040$ inch.

calculated ω-β diagrams. However, the effects of various loading dimensions on the ω-β diagram are correctly predicted by the theory, and the present analysis provides a reliable basis for an initial choice of design parameters.

It will be convenient to define $f(\pi)$ and $f(0)$ as the frequency at which $\theta = \pi$ and 0, respectively. For a forward-wave structure ($df/d\theta > 0$), $f(\pi) > f(0)$, and for the backward-wave structure ($df/d\theta < 0$) $f(\pi) < f(0)$.

In Fig. 6, calculated dispersion curves are shown for $W/L = 1.25$, $K(\pi)C(\pi)c/h = 0.05$ and various values of D/W. The frequency scale is normalized to $f_0(\pi)$, where $f_0(\pi)$ is the frequency of the empty comb ($D/W = 0$) at $\theta = \pi$. Without loading ($D/W = 0$), the structure is a forward-wave structure. Relatively thin slabs of ruby loading (see the curve for $D/W = 0.2$) make it a backward-wave structure of a comparatively wide bandwidth. This can be understood by observing that the RF fields near $\theta = \pi$ are more concentrated near the fingers than the RF fields near $\theta = 0$. Hence, the RF fields at $\theta = \pi$ see more of the presence of the thin ruby slab than the fields at $\theta = 0$. In this way $f(\pi)$ is reduced while $f(0)$ remains essentially unchanged. Further increases in the width of the loading (see the curves for $D/W = 0.4$ and 0.6) reduce the bandwidth of the backward-wave structure. This happens because the RF fields near $\theta = 0$ begin to interact with the dielectric slab, while the fields near $\theta = \pi$ are almost completely contained in the initial thin slabs. This again changes the frequencies at $\theta = \pi$ and 0 to a different extent and thus reduces $f(0)$ more than $f(\pi)$.

At a still greater dielectric slab thickness (see the curve for $D/W = 0.9$) the structure is forward with a fairly narrow band and finally, with complete loading (see the curve for $D/W = 1.0$), it is forward with a

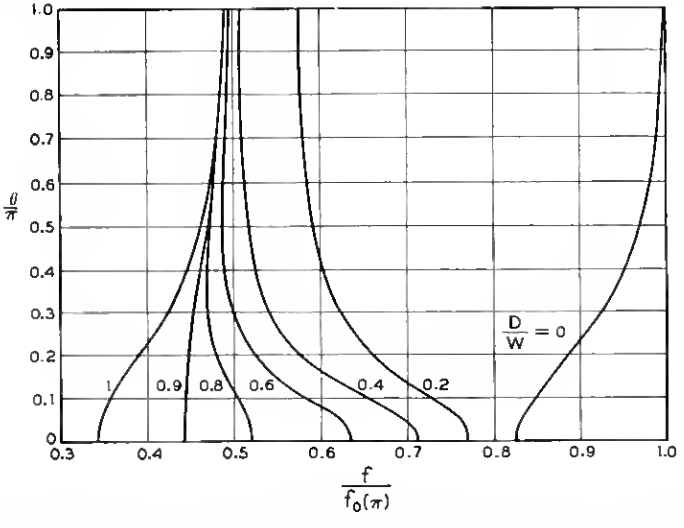

Fig. 6 — Calculated ω-β diagram as the thickness of the dielectric is changed. It is assumed that $L - l = l = d$, $W/L = 1.25$, $K(\pi)C(\pi)c/h = 0.05$, and $\epsilon = 9$. The frequency scale is normalized to $f_0(\pi)$, the frequency at $\theta = \pi$ for the empty comb.

somewhat wider band. The explanation is again based on the fact that increasing the dielectric width reduces the lower cutoff frequency while leaving the upper one the same.

The most important aspect of this behavior is seen by comparing the curves for $D/W = 0.6$, 0.8, and 0.9 in Fig. 6. It is apparent there that the transition between backward and forward structure does not involve baekward-wave structures of gradually decreasing bandwidth, and then forward-wave structures of initially very narrow and eventually wider bandwidths. If this were so, it would be very easy to design comb structures with extremely high slowing of the group velocity. Instead, it is seen that the transition from backward to forward-wave structures takes place via intermediate structures showing "fold-over." By this, we mean a structure whicb for some range of θ is forward, whereas it is backward in the remainder of the θ range. It has been pointed out[9] that such a situation leads to instability and oscillations in a traveling-wave maser amplifier in spite of the incorporated isolator. Thus, for all practical applications, the occurrence of fold-over has to be avoided.

It may be added here that dispersion curves of combs with other dimensions vary in a similar fashion as the thickness of the dielectric slab is varied. It is of interest, however, to find out how the onset of fold-over is related to the comb geometry, i.e., to the ratio W/L, and to the finger end capacity. Here it is particularly desirable to have analytical data which indicate what choice of the W/L and D/W ratios and of the finger end capacity will result in the greatest slowing of the group velocity near the center portion of the passband, but still avoid fold-over. For this purpose, a number of dispersion curves normalized to $f(\pi)$ were calculated and are shown in Fig. 7. One notices that fold-over takes place rather abruptly for $D/W \lesssim 0.9$ for all cases. In addition, one sees that the minimum group velocity $[\alpha(df/d\theta)]$ attainable near the center of the passband without fold-over decreases by reducing W/L and $\Delta h(\pi)/h$. The group velocity near the center of the passband is more or less arbitrarily defined as

$$v_g = L\,\frac{2\pi(f\,|_{\theta=0.7\pi} - f\,|_{\theta=0.3\pi})}{0.4\pi} \tag{19}$$

It is shown as a slowing factor $S \equiv c/v_g$ in Fig. 8 vs W/L for $D/W = 0.9$ and for different values of $\Delta h(\pi)/h$. The largest slowing is obtained for the smallest W/L. It should be pointed out, however, that our present calculations were not carried out for W/L ratios of 0.5 or smaller, although such values would increase the slowing still further. Values of $W/L \lesssim 0.5$ appear unsuitable for practical maser designs for various

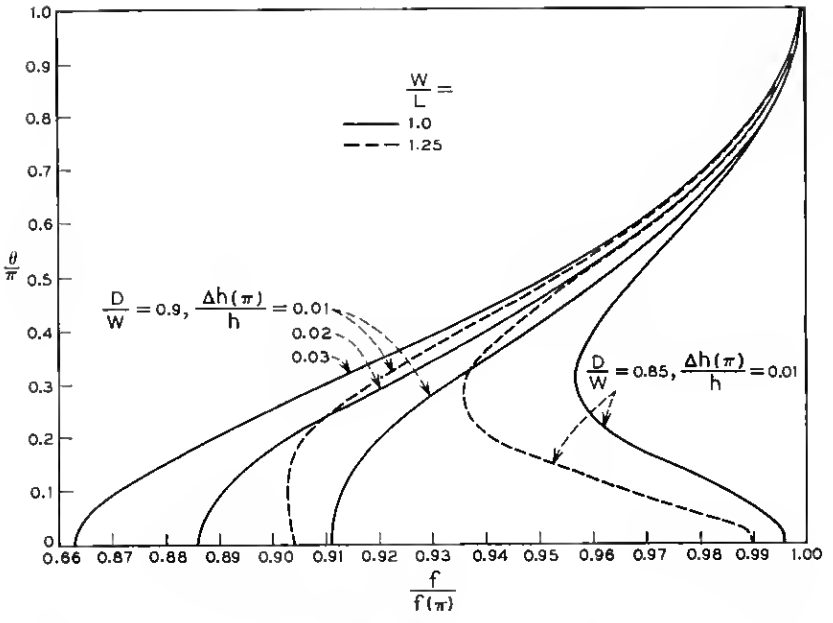

Fig. 7 — ω-β diagram for different W/L and $\Delta h(\pi)/h$. $D/W = 0.9$, $L - l = l = d$.

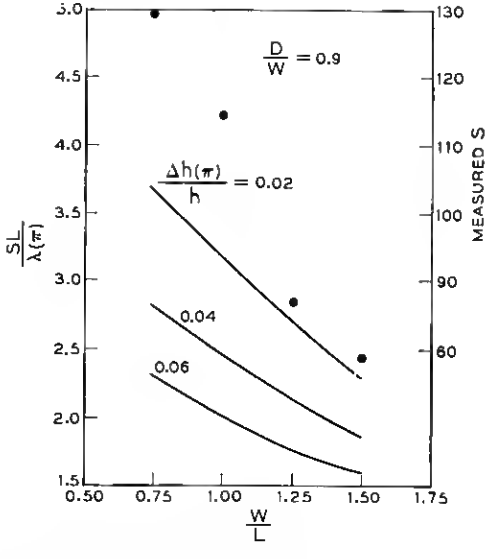

Fig. 8 — Slowing factor vs W/L. Measured points are also shown. The measurements are made with structures having $\Delta h/h = 0.02$, $\lambda(\pi) = 9.9$ cm, and $L = 0.08$ inch.

reasons, among them the difficulty of incorporating an isolator into a comb structure with such dimensions. Larger slowing results also from reducing $\Delta h(\pi)/h$. $\Delta h(\pi)$ can be varied over a narrow range by varying C, which is a function of s, the distance between the finger tip and the opposite waveguide wall. For the comb geometry used for measuring the fringe capacity, $C(\pi)$ does not appreciably decrease for s beyond $s \gtrsim 0.040$ inch. More generally, this would be done if s exceeds a value comparable to the finger "diameter." This therefore sets a minimum for $\Delta h(\pi)/h$ at a given operating frequency.

To illustrate the significance of Fig. 8, consider two TWM's A and B with exactly the same dimensions except that the finger length h of A is twice that of B. This difference in h makes the operating frequency of A about one-half of that of B. For the time being, assume also that the magnitude of the magnetic Q of the active crystal is independent of frequency. With the values $W/L = 1.0$ and $\Delta h(\pi)/h = 0.02$ for A, Fig. 8 shows that $SL/\lambda(\pi) = 3.2$. For B, $\Delta h(\pi)/h = 0.04$, so that $SL/\lambda(\pi) = 2.5$. The db gain of a TWM is proportional to fS/Q_m, which in turn, for constant Q_m, is proportional to $SL/\lambda(\pi)$. Thus one should expect that the db gain of maser A is larger than that of maser B by a factor 1.28 $(= 3.2/2.5)$. In practice, however, $|\, Q_m \,|$ usually increases toward lower frequencies, so that the gain of the lower-frequency maser A tends to be lower.

It should be added that the slowing itself, S, is inversely proportional to a scale factor $L/\lambda(\pi)$ where $\lambda(\pi) = c/f(\pi)$ is the free-space wavelength of $f(\pi)$. Thus for combs with a given period length L, the slowing is greater for lower frequencies. It follows that the slowing factor S is a meaningful parameter in comparing different comb structures only if they have essentially the same period length, L, and operating frequency range, f.

Consider another hypothetical case. Suppose the fringe capacity vanishes, $C(\pi) = C(0) = 0$, so that $\Delta h = 0$. Experimentally, this situation could be realized by a $\lambda/2$ ladder structure where fingers of twice the comb structure finger length are anchored at both ends in a waveguide enclosure. Without dielectric loading, this case would be that of the Easitron structure (see Ref. 7) which is characterized by a zero passband. With dielectric loading, however, a finite passband results nevertheless. This is due to the variation of $\epsilon(\theta)$ with θ, and in particular the difference between $\epsilon(\pi)$ and $\epsilon(0)$. Under these circumstances one might expect that the bandwidth is smaller and hence the slowing greater than in the case of a structure with finite fringe capacity and finite Δh. This is indeed the case. There is no curve shown in Fig. 8 for the parameter

$\Delta h = 0$, but it is obvious that this curve would lie above that for

$$\Delta h(\pi)/h = 0.02.$$

Measurements of dispersion curves of several comb structures loaded with alumina ($\epsilon = 9.3$) were made and they are shown in Fig. 9. Those parts of the dispersion curves where $\theta \geqq \pi/2$ depend very little on W/L and D/W. The fold-over takes place at D/W between 0.85 and 0.90. The maximum slowing factor near the center of the passband which is attainable without fold-over increases with smaller W/L. These general

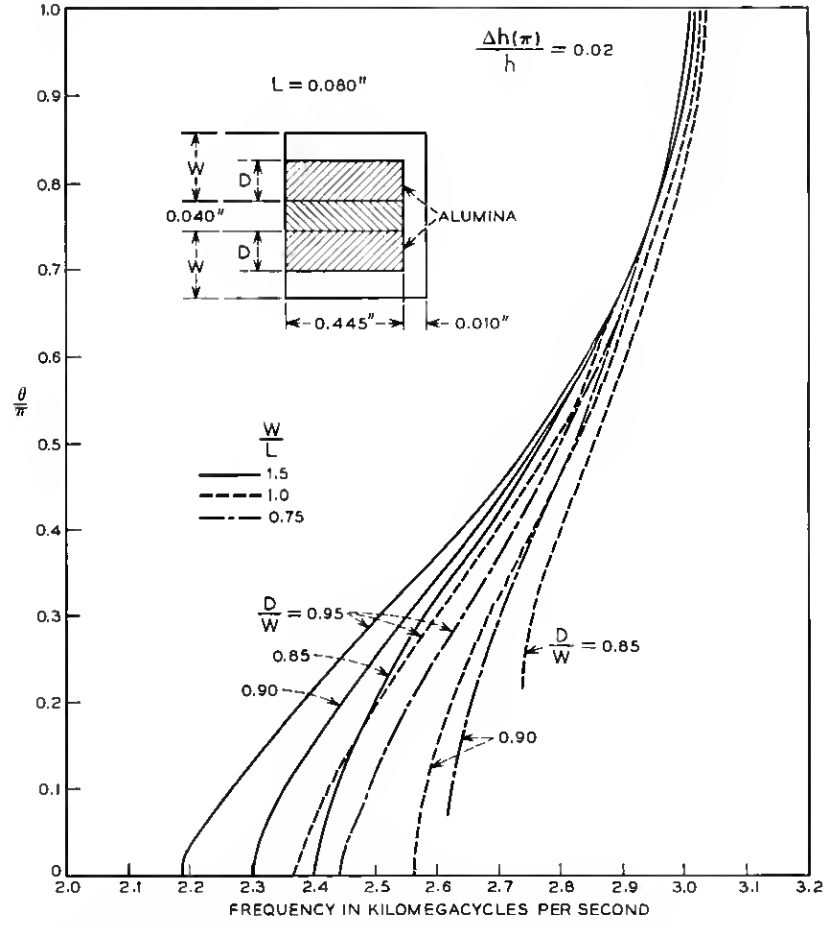

Fig. 9 — Measured ω-β diagrams of loaded comb structure. $L = l = l = d = 0.040$ inch.

features agree with the results of the calculation. There is a deviation of typically about 4 per cent near $\theta = \pi$, and of about 10 per cent near $\theta = 0$ between the absolute values of measured and calculated frequencies. These discrepancies are not too disturbing, however, since (3) is only an approximation; the fringe capacitance data derived for an empty comb change when the comb is loaded up to the tip of the fingers, and the dielectric constant of alumina is not exactly 9 as used in the calculations. The slowing factors calculated from these measurements are also shown in Fig. 8 as circled points. The measured slowing factors are about 30 per cent smaller than those calculated, but the dependence of S on W/L is correctly predicted by the theory.

VI. TECHNIQUES FOR REDUCING THE STRUCTURE BANDWIDTH

Since a structure with smaller bandwidth gives a larger slowing factor and thus a larger maser gain, the bandwidth of the structure should be kept as small as possible. It is necessary, of course, that the structure bandwidth exceed the required instantaneous or tunable design bandwidth of the maser amplifier by some reasonable, safe margin. This restriction was not important until recently. In earlier phases of traveling-wave maser development, it was difficult to design comb structures for sufficiently high slowing without running into the fold-over condition. More recently several techniques were developed which make it possible to design loaded comb structures with almost arbitrarily narrow bandwidths, down to structure bandwidths of only twice the instantaneous amplifier response.[5] These techniques were derived both by experimentation[10] and by the theoretical considerations reported in this paper. They include the following: (*i*) Near the tip of the fingers, the ruby may be shaped as in Fig. 10(a) or (b) by a step or bevel undercut. (*ii*) A strip of dielectric material of a high dielectric constant may be added next to the finger tips as in Fig. 10(c). (*iii*) The thickness of the comb fingers, d, may be reduced (see Fig. 1). These three techniques may be applied either independently or together to reduce the bandwidth of the structure.

By shaping the dielectric near the finger tip as in Fig. 10(a) and (b), the effective dielectric constant $\epsilon(\theta)$ is reduced. The reduction is not uniform across the band, but $\epsilon(\theta)$ is more drastically decreased for θ near 0. Thus, for a forward-wave structure where the lower cutoff frequency occurs at $\theta = 0$, the lower cutoff frequency increases without much change to the upper cutoff frequency. The bevel shape of Fig. 10(b) can be considered as a series of small steps, as indicated by the dashed line.

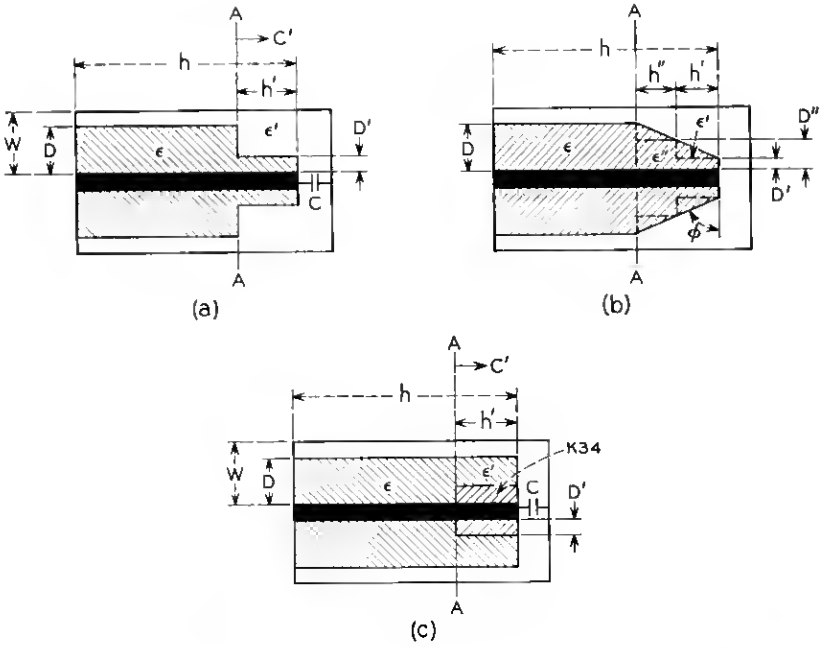

Fig. 10 — Techniques of "shaping" and "K34 loading" near the finger tip to reduce the bandwidth.

The dielectric shapes of Fig. 10(a) and (b) are approximately equivalent in their role of narrowing the bandwidth.

The finger tip loading may take the form shown in Fig. 10(c). A thin slab of dielectric material with high dielectric constant is imbedded in alumina or ruby near the finger tip. In our experiments, a ceramic with $\epsilon = 34$ manufactured by American Lava Corporation was used. This material will be referred to as K34. This type of finger tip loading increases the effective dielectric constant $\epsilon(\theta)$ near $\theta = \pi$ faster than near $\theta = 0$. For the forward-wave structure, this means that the upper cutoff frequency can be decreased faster than the lower cutoff frequency, and thus a narrowing of the bandwidth results.

Let h' be the length of the stepped dielectric (Fig. 10a) or K34 (Fig. 10c), C' be the capacitance looking toward the finger tip at the plane A-A, ϵ' be the effective dielectric constant of the section h', and D' be the thickness dimension as shown. The capacitive impedance looking toward the right side at the plane A-A, $1/\omega C'$, can be found by regarding the section h' as a TEM transmission line with the characteristic im-

pedance $K(\theta)/\sqrt{\epsilon'(\theta)}$ and a propagation constant $\omega\sqrt{\epsilon'(\theta)}/c$ and terminated by C at the end. If the electrical length of the modified section of finger line (which has the physical length h') is small compared to a quarter wavelength,

$$\tan \frac{\omega\sqrt{\epsilon'(\theta)}}{c} h' \approx \frac{\omega\sqrt{\epsilon'(\theta)}}{c} h',$$

and if the fringe capacity loading at the finger tip is small,

$$\frac{1}{\omega C} \gg \frac{K(\theta)}{\sqrt{\epsilon'(\theta)}}$$

then the effect of the stepped dielectric can be expressed by an effective capacity C'

$$C' \approx C[1 + (\epsilon' h'/KCc)] \tag{20}$$

which effectively terminates the regular TEM finger transmission lines of length h-h'. From (6) and (20) one obtains the following formula, which contains implicitly the ω-β relation

$$\frac{(2m-1)}{4}\lambda \approx \sqrt{\epsilon(\theta)}\left(h + \frac{KCc}{\epsilon} + \frac{\epsilon' - \epsilon}{\epsilon} h'\right). \tag{21}$$

For the stepped ruby as in Fig. 10(a) where $D > D'$, $(\epsilon' - \epsilon)/\sqrt{\epsilon}$ is negative. This quantity can be calculated from Fig. 3 and it is shown in Fig. 11 in solid curves. Measured values are also shown as circles. The measurements and calculations of $(\epsilon' - \epsilon)/\sqrt{\epsilon}$ agree well except near $\theta = 0$. In practical design work, it is often convenient to keep one of the cutoff frequencies unchanged while shifting the other cutoff frequency by shaping the dielectric. This requires a large ratio of

$$|(\epsilon' - \epsilon)/\sqrt{\epsilon}|$$

at the two cutoff frequencies. In Fig. 11, the curves for $D/W = 0.95$ and $0.4 \leqq D'/W \leqq 0.6$ satisfy this requirement. As a special case of stepped ruby, the value $D' = 0$ may also be considered. This corresponds to a ruby loading of rectangular cross section which does not cover the full finger height h. Then ϵ' becomes unity and the value $(1 - \epsilon)/\sqrt{\epsilon}$ is also plotted in Fig. 11 in the top curve marked $D'/W = 0.0$. Since the ratio $(1 - \epsilon)/\sqrt{\epsilon}$ at both cutoff frequencies, that is at $\theta = 0$ and at $\theta = \pi$, is not large, the reduction of the ruby height does not appear a promising way to narrow the bandwidth of the comb structure.

For K34 loading, $(\epsilon' - \epsilon)/\sqrt{\epsilon}$ becomes positive and can be evaluated

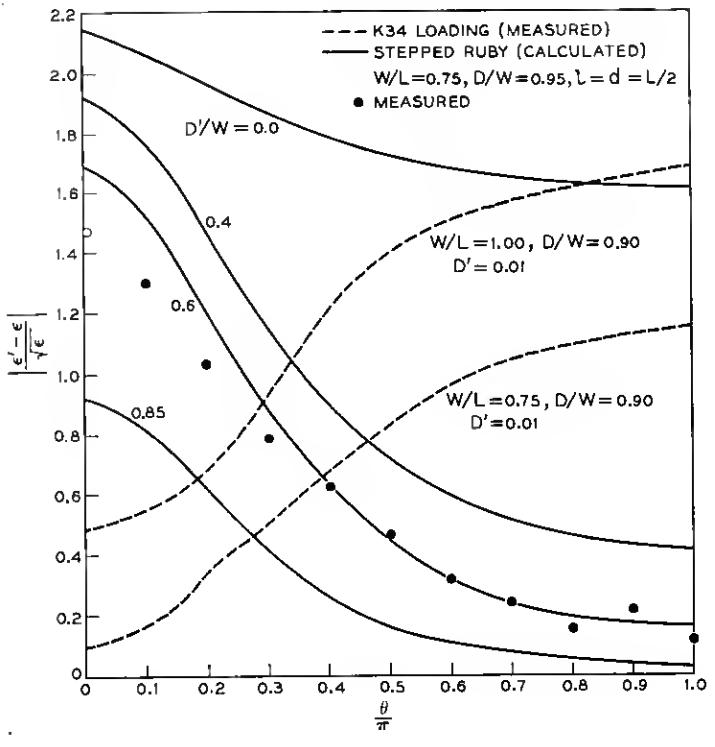

Fig. 11 — $\left|\frac{\epsilon' - \epsilon}{\sqrt{\epsilon}}\right|$ vs θ/π for ruby shaping and K34 loading.

from measured data with the help of (21). Two of the measured curves of $(\epsilon' - \epsilon)/\sqrt{\epsilon}$ are shown in Fig. 11 in broken lines. $(\epsilon' - \epsilon)/\sqrt{\epsilon}$ is larger near $\theta = \pi$ than near $\theta = 0$. For the forward-wave structure this causes the upper cutoff frequency to decrease while leaving the lower frequency almost unchanged.

The upper cutoff frequency of the forward-wave structure can also be reduced by using thin rectangular fingers (i.e., $d < L - l$). $\epsilon(\theta)$ of the comb structure with fingers of square cross section was shown in Fig. 3. It was also shown that $D/W = 0.9 \cdots 0.95$ is usually the best choice to reduce the bandwidth of the passband and yet avoid fold-over near $\theta = 0$. For this value of D/W, one notices in Fig. 3 that $\epsilon(0) > \epsilon(\pi)$. In order to reduce the bandwidth further, one may increase $\epsilon(\pi)$ so that it approaches $\epsilon(0)$. This can be done by reducing the dimension d of the fingers. Since the fields between the fingers are almost negligible at $\theta = 0$, the thickness dimension of the fingers does not affect $\epsilon(0)$. On

the other hand, near $\theta = \pi$ the fields see more of the ruby with thin fingers than with square fingers; thereby $\epsilon(\pi)$ increases.

In Fig. 12, $\sqrt{\epsilon(\pi)}$ vs $d/(L - l)$ using the expression given by Harris et al.[7] is shown. Three measured points are also indicated. The expression of $\epsilon(\pi)$ in Ref. 7 assumes a uniform field between the fingers. This approximation is less justified as the fingers become thin, although it should be qualitatively correct even for $d/(L - l) < 0.5$.

Both the K34 loading and the choice of finger thickness affect the frequencies near $\theta = \pi$. Band narrowing by thin fingers has the additional advantage that the filling factor improves somewhat compared to the use of K34 loading and of square fingers.

All the three techniques described here can be combined to narrow the passband very effectively in such a way that fold-over is still avoided.

VII. HIGHER-ORDER MODES

It has been shown in Section II that there exists a series of higher-order passbands for a comb structure.

Let us compare the first and the second modes of operation from two different approaches. Equation (6) shows that for a given θ the free-space wavelength of the first mode is three times longer than that of the second mode when all of the dimensions of the structure are kept the same. Thus the percentage bandwidth of the passbands is approximately the same for all modes. By using a frequency scale for the first mode which is

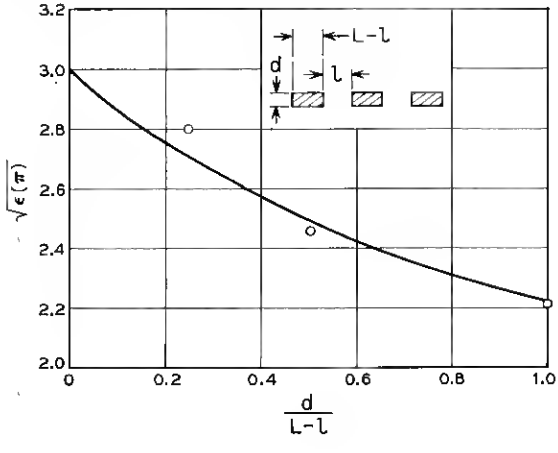

FIG. 12 — The square root of the effective dielectric constant at $\theta = \pi$ for "thin fingers." It is assumed that $\epsilon = 9$.

one-third that for the second mode, the ω-β diagram of the first and the second modes should coincide. This is indeed verified from measured ω-β diagrams of the first and the second modes of the structure designated as A in Fig. 13.

On the other hand, when W/L, D/W and s are kept unchanged while the length of the finger h is made three times longer, the passband of the smaller structure operating in its first mode will be in about the same frequency range as that of the larger structure operating in its second mode. However, the bandwidth of the smaller structure in the first mode is larger than that of the larger structure in the second mode. This is due to a larger $\Delta h/h$ for the structure with the smaller h. A structure B with a finger length of one-third that of structure A was built, and the ω-β diagram of its first mode is also shown in Fig. 13. One notices that the

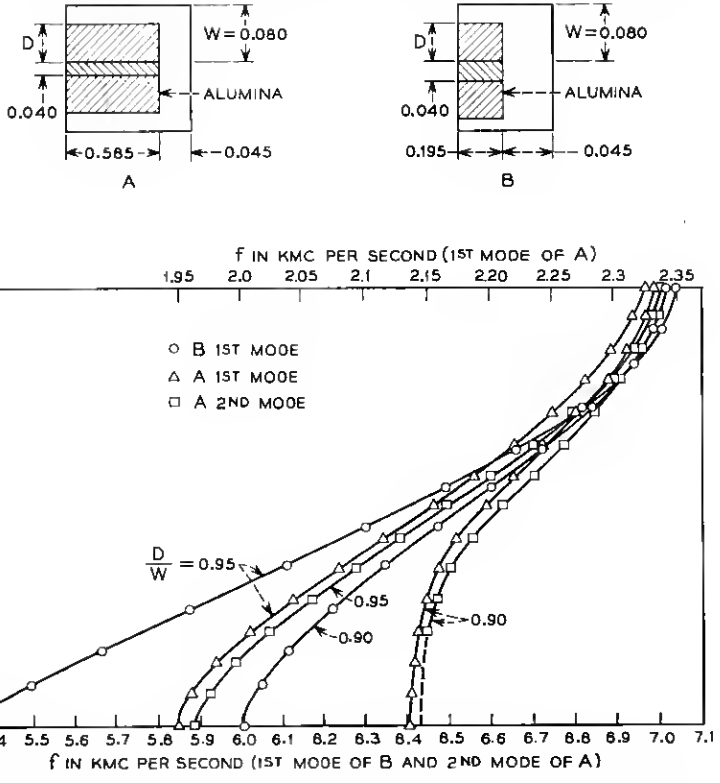

Fig. 13 — Comparisons of the first and the second passbands of the loaded comb structures. The fingers are 0.040 × 0.040 inch in cross section and l = 0.040 inch.

first mode of B has a larger bandwidth than the second mode of A. The larger slowing factor associated with the smaller bandwidth is one of the advantages of higher-order modes, but it is not an essential factor, since there are more efficient techniques of reducing the available bandwidth. However, the higher-order modes may be advantageous when the required microwave frequency of the passband is so high that it becomes difficult to fabricate comb fingers of a quarter-wave electrical length, provided the waveguide modes which may propagate in such a structure can be suppressed. Then the larger structure would permit reduced mechanical tolerances.

VIII. DESIGN CONSIDERATIONS

Since the gain of the maser increases as the bandwidth of the passband of the structure is reduced, it is preferable to design a structure having the narrowest bandwidth compatible with the requirements on the useful bandwidth of the maser.

The choice of various dimensions of the structure to obtain a given center frequency and to approach the narrowest bandwidth possible without fold-over will be discussed here.

From the curves in Fig. 8, a small value of W/L is preferred. Other design considerations may dictate the smallest permissible W/L value. In all our experiments, for example, a period length $L = 0.080$ inch was chosen. For W/L smaller than 0.7 it would seem rather difficult to incorporate a high-performance isolator into the structure. Thus $W/L \approx 0.7$ is a compromise optimum value.

With given dimensions of the empty comb and without ruby shaping near the finger tip, the bandwidth is reduced by gradually reducing D/W until fold-over sets in near $\theta = 0$. This happens at about $D/W \approx 0.9$. Fold-over appears more readily if additional "ruby shaping" is applied to the structure. Thus D/W should be larger than 0.9 in order to allow for some latitude in ruby shaping. From our experience $D/W = 0.95$ is a suitable value.

For the step in the ruby near the finger tip (Fig. 10a), D'/W may be taken between 0.4 and 0.6. Then $|(\epsilon' - \epsilon)/\sqrt{\epsilon}|$ at $\theta = 0$ is large, and the ratio of its magnitude at $\theta = 0$ and $\theta = \pi$ is also large.

The frequency near the $\theta = \pi$ end can be easily controlled by using thin fingers. The curve in Fig. 12 may serve as a guide in the choice of a suitable finger aspect ratio $d/(L - l)$.

The final parameter yet to be determined is the length of the fingers, h. For an initial design, one may use the midband value of $\sqrt{\epsilon}(\pi/2)$

from Fig. 3. Then

$$h \approx \frac{\lambda}{4\sqrt{\epsilon(\pi/2)}}$$

where λ is the free-space wavelength of the given center frequency. The three techniques discussed above for narrowing the bandwidth affect primarily the frequencies near $\theta = 0$ and $\theta = \pi$, i.e., close to both cutoffs; but the frequencies near $\theta = \pi/2$, i.e., close to midband, remain nearly unchanged.

Following the suggestions given here, one should arrive at a first-order design for a TWM which will perform fairly close to the theoretical expectation. Experience has shown that a small additional amount of fine adjustment is needed in order to have the traveling-wave maser perform according to the specifications. This may involve control of the center frequency, adjustment for more or less slowing in order to obtain the design gain, or adjustment of the curvature in the ω-β diagram so as to realize a flat gain-versus-frequency characteristic. The theoretical data provided in this paper make it rather easy to determine the appropriate design modifications.

IX. ACKNOWLEDGMENT

The author wishes to thank E. O. Schulz-DuBois for his helpful suggestions and critical reading of the manuscript. He also wishes to thank Mrs. E. Sonnenblick for the numerical computations and R. C. Peterson for the capacitance measurements in the electrolytic tank.

APPENDIX A

The Potential Distribution on the z Axis

Consider the coordinate axes shown in Fig. 14. The potential on the z axis for $-(l/2) < z < (l/2)$ can be expressed as

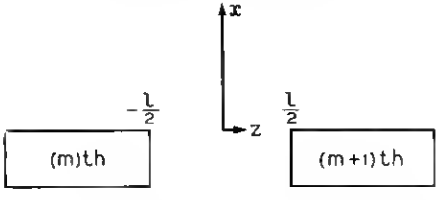

Fig. 14 The coordinate system used in Appendix A.

$$V(\theta,z) = V_s(\theta)g(z) + V_a(\theta)f(z) \tag{22}$$

where $V_s(\theta)$ and $V_a(\theta)$ are those parts of the potential which are symmetrical and antisymmetrical with respect to the x axis, respectively, and $g(z)$ and $f(z)$ describe their variation along the z axis. They are defined so that

$$g\left(-\frac{l}{2}\right) = g\left(\frac{l}{2}\right) = 1 \tag{23}$$

$$-f\left(-\frac{l}{2}\right) = f\left(\frac{l}{2}\right) = 1. \tag{24}$$

Substituting (23) and (24) into (22), the potentials of the mth and $(m + 1)$th finger become, respectively,

$$Ae^{-jm\theta} = V_s - V_a \tag{25}$$

$$Ae^{-j(m+1)\theta} = V_s + V_a. \tag{26}$$

From (25) and (26),

$$V_s = Ae^{-j(m+\frac{1}{2})\theta}\cos(\theta/2) \tag{27}$$

$$V_a = -jAe^{-j(m+\frac{1}{2})\theta}\sin(\theta/2). \tag{28}$$

Then (22) becomes

$$V(\theta,z) = Ae^{-j(m+\frac{1}{2})\theta}[g(z)\cos(\theta/2) - jf(z)\sin(\theta/2)]. \tag{29}$$

Assuming the fingers to be infinitely thin, $g(z)$ and $f(z)$ can be found from a Schwarz-Christoffel transformation. This transformation is described in Ref. 7. The result can be given in closed form for the derivatives $g' = dg/dz$ and $f' = df/dz$:

$$g' = \frac{\pi}{L\sqrt{\sin^2\dfrac{\pi z}{2l} - 0.5}} \frac{\cos\dfrac{\pi z}{2l}}{\dfrac{\pi W}{L} + \ln\sqrt{2}} \tag{30}$$

$$f' = \frac{\pi}{L\sqrt{\sin^2\dfrac{\pi z}{2l} - 0.5}} \frac{1}{1.854} \tag{31}$$

where it is assumed that $l/L = 0.5$. In deriving (30), an elliptic function has been approximated by a sine function. This approximation becomes better with larger W/L. The origin of the z coordinate for (30) and (31) is the same as originally indicated in Fig. 1, which differs from that shown

in Fig. 14. It is seen that an infinity occurs both for g' and f' at the finger corners, $z = \pm l/2$.

APPENDIX B

Impedance of a Finger Based on the "Thin-Tape" Approximation

It was shown in Section III that the admittance of a finger can be found by adding the admittance between the fingers Y_1, and the admittance between the finger and the waveguide Y_2. Y_2 can be expressed in terms of the potentials f and g along the z axis of Fig. 14. f and g are the potentials at $\theta = \pi$ and $\theta = 0$, respectively. We shall assume f and g to be those obtained by conformal mapping of the thin-tape geometry.

By separating the term with $n = 0$ from the remaining summation, (13) may be rewritten in the following form

$$\frac{Y_2(\theta)}{Y_0} \doteq \frac{\sin\frac{\theta}{4}}{\frac{\theta}{4}} \coth\left(\theta\frac{W}{L}\right) \times \frac{2}{L}\left[\sin\frac{\theta}{2}\int_{-l/2}^{l/2} f' \cos\frac{\theta}{L}z\,dz + \cos\frac{\theta}{2}\int_{-l/2}^{l/2} g' \sin\frac{\theta z}{L}\,dz\right] + \sum_{\substack{n=-\infty \\ n\neq 0}}^{\infty} (-1)^{n+r} \cdot \frac{\sin\left(\frac{\theta}{4}+\frac{n\pi}{2}\right)}{\frac{\theta}{4}+\frac{n\pi}{2}} \left(\sin\frac{\theta}{2}\right)\frac{2}{L}\int_{-l/2}^{l/2} f' \cos(\theta + 2n\pi)\,\frac{z}{L}\,dz \tag{32}$$

for

$$L - l = l = d$$

where

$$r = 0 \quad \text{for} \quad n > 0$$

$$r = 1 \quad \text{for} \quad n < 0.$$

The terms involving g are omitted except for $n = 0$, since usually $g' \ll f'$. The coordinate origin used in this equation is at the position shown in Fig. 14.

Let Y_L, Y_M and Y_U be $Y_2(\theta)/Y_0$ at $\theta = 0$, $\pi/2$ and π, respectively. These quantities can be obtained directly by conformal mapping. Y_L and Y_U are shown in Ref. 7. Y_M is obtained by a similar procedure and

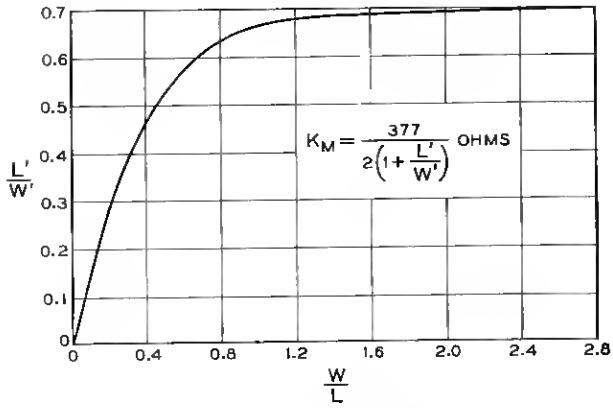

Fig. 15 — The impedance $K(\theta)$ of a finger at $\theta = \pi/2$.

the result is shown in Fig. 15. For θ other than these three values, (32) should in principle be used to find $Y_2(\theta)$. Fortunately, $Y_2(\theta)$ can be expressed approximately in terms of Y_L and Y_M or Y_U in an interpolation formula, and thus the tedious evaluation of (32) can be avoided.

Letting $\theta = 0$ and then $\theta = \pi/2$ in (32), one obtains,

$$Y_L = \frac{1}{W}\left[\int_{-l/2}^{l/2} f'\,dz + \frac{2}{L}\int_{-l/2}^{l/2} zg'\,dz\right] \tag{33}$$

$$Y_M = \frac{\sin\frac{\pi}{8}}{\frac{\pi}{8}} \coth\frac{\pi W}{2L}\left(\sin\frac{\pi}{4}\right)\frac{2}{L}\left[\int_{-l/2}^{l/2} f' \cos\frac{\pi z}{2L}\,dz + \int_{-l/2}^{l/2} g' \sin\frac{\pi z}{2L}\,dz\right] + \frac{2}{L}\sum_{\substack{n=-\infty \\ n\neq 0}}^{\infty}(-1)^{n+r} \cdot \frac{\sin\left(\frac{\pi}{8}+\frac{n\pi}{2}\right)}{\frac{\pi}{8}+\frac{n\pi}{2}} \sin\frac{\pi}{4}\int_{-l/2}^{l/2} f' \cos\left(\frac{\pi}{2}+2n\pi\right)\frac{z}{L}\,dz. \tag{34}$$

We shall assume that approximately

$$\int_{-l/2}^{l/2} f'\,dz \doteq \int_{-l/2}^{l/2} f' \cos\frac{\theta z}{L}\,dz \tag{35}$$

$$\frac{\sin\left(\frac{\theta}{4}+\frac{n\pi}{2}\right)}{\frac{\theta}{4}+\frac{n\pi}{2}} \doteq \frac{\sin\left(\frac{\pi}{8}+\frac{n\pi}{2}\right)}{\frac{\pi}{8}+\frac{n\pi}{2}}, \qquad \text{for } n \neq 0 \quad (36)$$

$$\int_{-l/2}^{l/2} f' \cos(\theta + 2n\pi)\frac{z}{L}\,dz \doteq \int_{-l/2}^{l/2} f' \cos\left(\frac{\pi}{2}+2n\pi\right)\frac{z}{L}\,dz, \qquad \text{for } n \neq 0 \quad (37)$$

$$\int_{-l/2}^{l/2} g' \sin\frac{\theta z}{L}\,dz \doteq \frac{2}{L}\int_{-l/2}^{l/2} g'\,z\,dz. \quad (38)$$

Then (32) becomes

$$Y_2(\theta) \doteq \frac{\sin\frac{\pi}{2}}{\sin\frac{\pi}{4}} Y_M + \left(\frac{\sin\frac{\theta}{4}}{\frac{\theta}{4}}\coth\theta\frac{W}{L} - \frac{\sin\frac{\pi}{8}}{\frac{\pi}{8}}\coth\frac{\pi W}{2L}\right)\frac{2W}{L} \cdot\sin\frac{\theta}{2}\,Y_L + \frac{\sin\frac{\theta}{4}}{\frac{\theta}{4}}\left(\coth\theta\frac{W}{L}\right)\left(\cos\frac{\theta}{2}-\sin\frac{\theta}{2}\right)\frac{4}{L^2}\int_{-l/2}^{l/2} g'\,z\,dz. \quad (39)$$

The last term of (39) is small compared to the other terms, and it can be found by numerical integration of g' in (30).

One notices that $Y_2(\theta)$ of (39) becomes Y_L and Y_M when $\theta = 0$ and $\theta = \pi/2$, respectively. One may estimate the error involved in (39) by letting $\theta = \pi$ and compare it with Y_U obtained by conformal mapping. For $W/L = 1$, $Y_2(\pi)$ obtained from (39) gives a value 10 per cent smaller than that obtained directly by conformal mapping. The admittance of a finger which is the sum of Y_1 and Y_2 thus has an error of about 4 per cent at $\theta = \pi$. For other values of θ, the error would be even smaller.

REFERENCES

1. DeGrasse, R. W., Schulz-DuBois, E. O., and Scovil, H. E. D., The Three-Level Solid-State Traveling-Wave Maser, B.S.T.J., **38**, Mar., 1959, pp. 305–334.
2. Fletcher, R. C., A Broadband Interdigital Circuit for Use in Traveling-Wave Tube Amplifiers, Proc. I.R.E., **40**, Aug., 1952, pp. 951–958.
3. Butcher, P. N., The Coupling Impedance of Tape Structures, J. IEE, **104B**, Mar., 1957, pp. 177–187.
4. Walling, J., Interdigital and Other Slow Wave Structures, J. Electronics, **3**, Mar., 1957, pp. 239–258.
5. Ash, E. A., and Studd, A. C., A Ladder Structure for Millimeter Waves, I.R.E. Trans. Electron Devices, **ED-8**, July, 1961, pp. 294–302.

6. Tabor, W. J., A 100-Mc Broadband Ruby Traveling-Wave Maser at 5 Gc, Proc. IEEE, **51**, August, 1963, p. 1143.
7. Harris, S., DeGrasse, R. W., and Schulz-DuBois, E. O., Cutoff Frequencies of the Dielectrically Loaded Comb Structure as Used in Traveling-Wave Masers, B.S.T.J., **43**, Jan., 1964, p. 437.
8. Haddad, G. I., and Rowe, J. E., X-Band Ladder-Line Traveling-Wave Maser, I.R.E. Trans. on Microwave Theory and Techniques, **MTT-10**, January 1962, pp. 3–8.
9. Kostelnik, J. J., DeGrasse, R. W., and Scovil, H. E. D., The Dual Channel 2390-mc Traveling-Wave Maser, B.S.T.J., **40**, July, 1961, pp. 1117–1127.
10. DeGrasse, R. W., and Hensel, M. L., private communication.